Ab Initio Calculations on the Mechanism of the Oxidation of the Hydroxymethyl Radical by Molecular Oxygen in the Gas Phase: A Significant Reaction for Environmental Science

Santiago Olivella,*[a] Josep M. Bofill,[b] and Albert Solé[c]

Abstract: The mechanism of the gas-phase reaction of $^{\cdot}CH_2OH+O_2$ to form $CH_2O+HO_2^{\cdot}$ was studied theoretically by means of high-level quantum-chemical electronic structure methods (CASSCF and CCSD(T)). The calculations indicate that the oxidation of $^{\cdot}CH_2OH$ by O_2 is a two-step process that goes through the peroxy radical intermediate $^{\cdot}OOCH_2OH$ (**1**), formed by the barrier-free radical addition of $^{\cdot}CH_2OH$ to O_2. The concerted elimination of $HO_2^{\cdot}$ from **1** is predicted to occur via a five-membered ringlike transition structure of C_s symmetry, **TS1**, which lies 19.6 kcal mol^{-1} *below* the sum of the energies of the reactants at 0 K. A four-membered ringlike transition structure **TS2** of C_s symmetry, which lies 13.9 kcal mol^{-1} above the energy of the separated reactants at 0 K, was also found for the concerted $HO_2^{\cdot}$ elimination from **1**. An analysis of the electronic structures of **TS1** and **TS2** indicates that both modes of concerted $HO_2^{\cdot}$ elimination from **1** are better described as internal proton transfers than as intramolecular free-radical H-atom abstractions. The intramolecular 1,4-H-atom transfer in **1**, which yields the alkoxy radical intermediate $HOOCH_2O^{\cdot}$, takes place via a puckered ringlike transition structure **TS3** that lies 13.7 kcal mol^{-1} above the energy of the reactants at 0 K. In contrast with earlier studies suggesting that a direct H-atom abstraction mechanism might occur at high temperatures, we could not find any transition structure for direct H-atom transfer from the OH group of $^{\cdot}CH_2OH$ to the O_2. The observed non-Arrhenius behavior of the temperature dependence of the rate constant for the gas-phase oxidation of $^{\cdot}CH_2OH$ is ascribed to the combined effect of the initial barrier-free formation of the $^{\cdot}OOCH_2OH$ adduct with a substantial energy release and the existence of a low-barrier and two high-barrier pathways for its decomposition into CH_2O and $HO_2^{\cdot}$.

Keywords: ab initio calculations · atmospheric chemistry · hydrogen transfer · radicals · reaction mechanisms

Introduction

The hydroxymethyl radical ($^{\cdot}CH_2OH$) has been shown to be important in the chemistry that occurs in polluted atmospheres as it is a final product of a series of reactions initiated by the reaction of hydroxyl radical ($HO^{\cdot}$) with ethylene.[1] Thus $^{\cdot}CH_2OH$ plays a key role in the chemistry of the polluted stratosphere and troposphere.[2] The principal fate of this radical under atmospheric conditions is reaction with molecular oxygen (O_2, $^3\Sigma_g^-$) to form formaldehyde (CH_2O) and hydroperoxy radical ($HO_2^{\cdot}$) [Eq. (1)]. This reaction also is

$$^{\cdot}CH_2OH+O_2 \longrightarrow CH_2O+HO_2^{\cdot} \quad (1)$$

important in combustion chemistry (e.g., in methanol flames).[3] Several groups reported rate constant measurements for reaction (1). Dóbé et al.,[4] Grotheer et al.,[5] Payne et al.,[6] and Nesbitt et al.[7] obtained a rate constant of 9.0×10^{-12} cm^3 molecule^{-1} s^{-1} at 298 K, with an estimated overall uncertainty of +30%. Grotheer et al.[5b] and Nesbitt et al.[7] have studied the temperature dependence of the rate constant for this reaction. A strong non-Arrhenius behavior was

[a] Prof. S. Olivella[+]
Centre de Recerca en Química Teòrica
Martí i Franquès 1, 08028 Barcelona, Catalonia (Spain)
E-mail: olivella@qo.ub.es

[b] Dr. J. M. Bofill
Centre de Recerca en Química Teòrica and
Departament de Química Orgànica
Universitat de Barcelona, Martí i Franquès 1
08028 Barcelona, Catalonia (Spain)

[c] Dr. A. Solé
Centre de Recerca en Química Teòrica and
Departament de Química Física
Universitat de Barcelona, Martí i Franquès 1, 08028 Barcelona, Catalonia (Spain)

[+] Institut d'Investigacions Químiques i Ambientals de Barcelona, CSIC
Jordi Girona 18, 08034 Barcelona, Catalonia (Spain)
Fax: (+34) 93-3397878

Supporting information for this article (Tables S1–S6, which summarize total energies, relative energies, zero-point vibrational energies, thermal corrections to enthalpy, and absolute entropies, calculated at different levels of theory of all structures reported in this paper. It also includes a Figure showing the optimized geometries of O_2, $^{\cdot}CH_2OH$, $HO_2^{\cdot}$, and CH_2O) is available on the WWW under http://www.chemistry/home/ or from the author.

  0947-6539/01/0715-3377 $ 17.50+.50/0

observed, with the rate constant decreasing below room temperature and also decreasing slightly above room temperature, with a minimum at ≈400–450 K. These observations were explained on the basis of different mechanisms for the high-temperature and low-temperature reactions.[7]

The lack of an isotope effect on the room temperature rate constant for the reactions of the $^{\cdot}CH_2OH$ and $^{\cdot}CH_2OD$ radicals with molecular oxygen[5b] and the temperature dependence of the rate constant for the 215–250 K interval[7] were interpreted as an indication that reaction (1) proceeds by initial radical addition of $^{\cdot}CH_2OH$ to O_2 to form the peroxy radical $^{\cdot}OOCH_2OH$ (**1**) as intermediate [Eq. (2)]. This can then dissociate back to reactants or undergo an intramolecular 1,4-hydrogen shift, via a five-membered transition state, to form the alkoxy radical $HOOCH_2O^{\cdot}$ (**2**) [Eq. (3)], which in turn readily decomposes to form the observed products CH_2O and $HO_2^{\cdot}$ [Eq. (4)]. In addition to this addition/rearrangement/decomposition pathway, reaction (1) could also occur by a bimolecular hydrogen abstraction mechanism through direct transfer of the H atom of the OH group to the O_2.[5b, 7] This would be expected to be important at high temperatures if there is a substantial activation energy.

$$^{\cdot}CH_2OH + O_2 \longrightarrow {}^{\cdot}OOCH_2OH \quad (2)$$

$$^{\cdot}OOCH_2OH \longrightarrow HOOCH_2O^{\cdot} \quad (3)$$

$$HOOCH_2O^{\cdot} \longrightarrow CH_2O + HO_2^{\cdot} \quad (4)$$

Abstract in Catalan: *El mecanisme de la reacció en fase gasosa $^{\cdot}CH_2OH+O_2$ conduint a $CH_2O+HO_2^{\cdot}$ va ser estudiat teòricament emprant mètodes químico-quàntics de càlcul de l'estructura electrònica d'alt nivell (CASSCF i CCSD(T)). Els càlculs indiquen que l'oxidació del $^{\cdot}CH_2OH$ pel O_2 és un procés en dues etapes que té lloc a través de l'intermediari radical peroxi $^{\cdot}OOCH_2OH$ (**1**), format per l'addició radicalària del $^{\cdot}CH_2OH$ al O_2 sense cap barrera. Es prediu que l'eliminació concertada del $HO_2^{\cdot}$ des de **1** té lloc a través d'una estructura de transició de cinc baules de simetria C_s **TS1**, situada a 19.6 kcal mol^{-1} per sota de la suma de les energies dels reactius a 0 K. Per l'eliminació concertada del $HO_2^{\cdot}$ des de **1** també es va trobar una estructura de transició de quatre baules de simetria C_s **TS2**, situada a 13.9 kcal mol^{-1} per sobre l'energia dels reactius separats a 0 K. Una anàlisi de l'estructura electrònica de **TS1** i **TS2** indica que ambdues maneres d'eliminació del $HO_2^{\cdot}$ des de **1** es descriuen millor com a transferències protòniques internes que no pas substraccions radicalàries intramoleculars de H. La transferència intramolecular 1,4 de H a **1**, per a donar l'intermediari radical alcoxi $HOOCH_2O^{\cdot}$, té lloc a través de l'estructura de transició de tipus anell arrugat **TS3**, situada a 13.7 kcal mol^{-1} per sobre de l'energia dels reactius a 0 K. Contrariament a estudis anteriors que suggereixen un mecanisme de substracció directa de H a altes temperatures, no es va trobar cap estructura de transició per a la transferència directa de H des del grup OH del $^{\cdot}CH_2OH$ cap el O_2. El comportament no-Arrhenius de la dependència de la constant de velocitat amb la temperatura, per l'oxidació del $^{\cdot}CH_2OH$ en fase gasosa, s'atribueix a un efecte combinat de la formació de l'adducte $^{\cdot}OOCH_2OH$ sense cap barrera amb un alliberament d'energia substancial i l'existència d'un camí de reacció amb una barrera baixa i dos camins de reacció amb barreres altes per la seva descomposició en CH_2O i $HO_2^{\cdot}$.*

Under tropospheric conditions, the above addition/rearrangement/decomposition mechanism is generally accepted.[2] However, it is worth noticing that the radical addition of $HO_2^{\cdot}$ to CH_2O in the gas phase is known to yield the peroxy radical intermediate **1** [Eq. (5)].[8] By using both MP4 and BAC MP4

$$CH_2O + HO_2^{\cdot} \longrightarrow {}^{\cdot}OOCH_2OH \quad (5)$$

(bond additivity correction at MP4 level)/6-31G(d,p) ab initio calculations at geometries optimized at the UHF/6-31G(d) level, Evleth et al.[9] have investigated the mechanism of reaction (5). The first structure encountered on the reaction path taking $CH_2O+HO_2^{\cdot}$ to **1** was a hydrogen-bonded complex between CH_2O and $HO_2^{\cdot}$, which is formed with a computed reaction enthalpy at 300 K on the order of -8 kcal mol^{-1} without an activation energy. This $CH_2O\cdots HO_2^{\cdot}$ complex rearranges directly to give the product **1** via a planar five-membered transition structure involving the simultaneous addition of the terminal oxygen of $HO_2^{\cdot}$ to the carbon atom of the CO bond and transfer of a proton to the oxygen of this same bond. The 300 K barrier for this rearrangement was predicted to be 1.3 kcal mol^{-1} at the BAC-MP4/6-31G(d,p) level. Evleth et al.[9] also located a transition structure connecting $CH_2O+HO_2^{\cdot}$ to **2**. At the BAC-MP4/6-31G(d,p) level, the 300 K heat of formation of this transition structure was computed to be 24.6 kcal mol^{-1} higher than that computed for the transition structure connecting the $CH_2O\cdots HO_2^{\cdot}$ complex to **1**. Thus it was concluded that probably no alkoxy radical intermediate **2** is formed in this reaction. This conclusion calls into question the validity of the generally accepted addition/rearrangement/decomposition mechanism [Eq. (2)–(4)] for reaction (1) under tropospheric conditions as concerns the intermediacy of radical **2**.

In summary, we feel that there is a need for high-level quantum-chemical calculations of the potential energy surface (PES) of the $^{\cdot}CH_2OH+O_2$ reaction, in order to elucidate the mechanism by which CH_2O and $HO_2^{\cdot}$ are formed and to ascertain the nature of the transition state involved. For this purpose, we present the results of our theoretical investigation. Specifically, we report a complete characterization of nine stationary points on the ground-state PES of the $^{\cdot}CH_2OH+O_2$ reaction, including predictions of geometric structures, harmonic vibrational frequencies, absolute entropies, and relative energies of minima and transition structures. Energy differences between three different stepwise addition/elimination mechanisms are obtained and rationalized in terms of the structural features shown by the radical intermediates and transition structures involved.

Methods and Computational Details

The geometries of the relevant stationary points on the ground-state PES of the $^{\cdot}CH_2OH+O_2$ reaction were initially optimized by using the spin-

0947-6539/01/0715-3378 $ 17.50+.50/0 *Chem. Eur. J.* **2001**, *7*, No. 15

unrestricted Hartree–Fock (UHF) version of the self-consistent field (SCF) molecular orbital (MO) method[10] with the d-polarized split-valence 6-31G(d) basis set[11] employing analytical gradient procedures.[12, 13] All of these ab initio calculations were performed with the Gaussian 94 program package.[14]

The UHF wave function of some calculated transition structures (**TS3** and **TS4;** see Figures 7 and 9) was subjected to serious spin contamination, indicating strong nondynamic electron correlation effects. One may then question the reliability of the geometries calculated at the UHF level of theory for these structures. Consequently, all of the geometries (minima and saddle points) were reoptimized by use of multiconfiguration SCF (MCSCF) wave functions of the complete active space (CAS) SCF class[15] with the d,p-polarized triple split-valence 6-311G(d,p)[16] basis sets with analytical gradient procedures.[13, 17] The CASs were selected following the procedure suggested by Anglada and Bofill,[18] based on the fractional occupation of the natural orbitals generated from the first-order density matrix calculated from an initial multireference single- and double-excitation configuration interaction (MRDCI) wave function correlating all valence electrons. All CASSCF geometry optimizations were carried out by using the GAMESS system of programs.[19]

All the stationary points were characterized by their harmonic vibrational frequencies as minima or saddle points. The harmonic vibrational frequencies were obtained by diagonalizing the mass-weighted Cartesian force constant matrix calculated analytically at the CASSCF level of theory with the 6-311G(d,p) basis set by using Gaussian 94. Connections of the transition structures between designated minima were confirmed by intrinsic reaction coordinate (IRC)[20] calculations at the CASSCF/6-311G(d,p) level with the second-order algorithm of Gonzalez and Schlegel[21] implemented into GAMESS, with a step size of 0.15 bohr amu$^{1/2}$.

With the aim of assessing the performance of current density functional theory (DFT) for the description of intramolecular free-radical H-atom abstractions in oxygen-centered radicals, geometries and harmonic vibrational frequencies of the stationary points located on the CASSCF PES were also calculated. For this we used the spin-unrestricted version of the Becke three-parameter hybrid functional[22] combined with the Lee, Yang, and Parr (LYP) correlation functional,[23] designated UB3LYP,[24] employing the 6-311G(d,p) basis set. Two transition structures (**TS2** and **TS3**) proved to be problematic for the UB3LYP method. For that reason, we also calculated the geometries and harmonic vibrational frequencies of the most relevant stationary points on the CASSCF PES by using second-order Møller–Plesset perturbation theory (MP2)[25] and the configuration interaction with all single and double excitations (CISD)[26] method, based on a reference UHF single determinant, designated UMP2 and UCISD, respectively. Both the UMP2 and UCISD calculations were performed with core electrons excluded from the correlation treatment (frozen core approximation), with the 6-311G(d,p) basis set.

To incorporate the effect of dynamic valence-electron correlation on the relative energy ordering of the stationary points located at the CASSCF/6-311G(d,p) level, we carried out single-point (frozen core) coupled-cluster[27] calculations including all single and double excitations, together with a perturbative treatment of all connected triple excitations[28] (CCSD(T)), based on a reference UHF single determinant, designated UCCSD(T). To establish that our results converged with respect to the basis set, both the UCCSD(T) and UB3LYP calculations were carried out with the 6-311G(d,p) basis set; the 6-311 + G(d,p) basis set[29] (which includes a single additional diffuse sp shell on heavy atoms only); the 6-311 + G(3df,2p) basis set[29] (which includes triple d-polarization and a single additional f-polarization on heavy atoms and double p-polarization on hydrogen atoms); and the Dunning correlation-consistent polarized valence triple-ζ [10s5p2d1 f/4s3p2d1 f] basis set for carbon and oxygen, and [5s2p1d/3s2p1d] for hydrogen, designated cc-pVTZ.[30] Finally, total energies for the stationary points were also evaluated from partially spin-adapted CCSD(T) calculations based on a restricted open-shell Hartree–Fock reference determinant (RCCSD(T)[31]) to overcome the spin contamination problem in UCCSD(T) wave functions.[32] Unless otherwise noted, relative energies in the text refer to the RCCSD(T)/cc-pVTZ level of computation. The UMP2, UCISD, UB3LYP, and UCCSD(T) calculations were carried out with Gaussian 94, whereas the MOLPRO 98[33] program package was employed for the RCCSD(T) calculations.

Zero-point vibrational energies (ZPVE) were determined from unscaled harmonic vibrational frequencies calculated at the CASSCF/6-311G(d,p) level. Our best total energies at 0 K correspond to the sum of the RCCSD(T)/cc-pVTZ energy and ZPVE correction. Thermal corrections to enthalpy, absolute entropies, and Gibbs free-energy values were obtained assuming ideal gas behavior from the unscaled harmonic frequencies and moments of inertia by standard methods.[34] A standard pressure of one atmosphere was used in the absolute entropy calculations.

To examine the characteristics of the bonding and interactions in the most relevant structures we have also performed an analysis of the electronic charge density within the framework of the topological theory of atoms in molecules (AIM)[35] making use of the PROAIM and EXTREME programs of Bader et al.[36] and the MORPHY 97 program.[37] The first-order electron density matrix obtained from the CASSCF/6-311G(d,p) wave function was used in this analysis.

Results and Discussion

Energetics of the oxidation of the hydroxymethyl radical by molecular oxygen: Figure 1 summarizes the potential energy profiles calculated at the RCCSD(T)/cc-pTZ+ZPVE level for the different pathways found on the CASSCF PES for this reaction. According to Table 1, reaction (1) is predicted to involve a 0 K energy of reaction (ΔE_r(0 K)) of -18.8 kcal mol^{-1}. Inclusion of the thermal correction to enthalpy (ΔH_c(298 K)) leads to a 298 K enthalpy of reaction (ΔH_r(298 K)) of -18.7 kcal mol^{-1}, which is in good agreement with the value of -18.1 ± 1.0 kcal mol^{-1} obtained from experimental enthalpies of formation at this temperature.[39] The UB3LYP/cc-pVTZ calculations (Table 2) predict a ΔH_r(298 K) of -17.1 kcal mol^{-1}.

Initial reaction of hydroxymethyl radical with molecular oxygen: As shown in Figure 1, the first step of the $^{\bullet}CH_2OH+O_2$ ($^3\Sigma_g^-$) reaction is the formation of the peroxy radical **1** without surmounting an energy barrier. This result is in good general agreement with ab initio quantum-chemical[43] and DFT[44–46] calculations, which show that the reaction of methyl radical with O_2 ($^3\Sigma_g^-$) starts with the formation of methylperoxy radical $CH_3OO^{\bullet}$ with no energy barrier. Selected geometric parameters of the equilibrium structure calculated for **1** are shown in Figure 2. At the CCSD(T)/cc-pVTZ+ZPVE level of computation (Table 1), the formation of **1** from $^{\bullet}CH_2OH+O_2$ is predicted to be exoergic by 32.5 kcal mol^{-1}. Inclusion of ΔH_c(298 K) leads to a ΔH_r(298 K) of -33.9 kcal mol^{-1}. Notably, at the CCSD(T)/cc-pVTZ+ZPVE level the energy of **1** lies 13.7 kcal mol^{-1} below the sum of the energies of CH_2O and $HO_2^{\bullet}$. After inclusion of ΔH_c(298 K) this energy difference increases to 15.2 kcal mol^{-1}. The latter value is in reasonable agreement with the experimental ΔH_r(300 K) of -16.3 kcal mol^{-1} reported for reaction (5).[8] Regarding the UB3LYP calculations (Table 2), we note that at the UB3LYP/cc-pVTZ+ZPVE level **1** is predicted to lie 30.2 kcal mol^{-1} below the sum of the energies of the reactants $^{\bullet}CH_2OH+O_2$ and 13.1 kcal mol^{-1} below that of the products $CH_2O+HO_2^{\bullet}$. From the ΔH(298 K) given in Table 2, a ΔH_r(298 K) of -14.5 kcal mol^{-1} is obtained for reaction (5). This value is 1.8 kcal mol^{-1} higher than the reported experimental ΔH_r(300 K). Regarding the entropy change at 298 K (ΔS_r(298 K)) for reaction (5), the values of -38.3 and

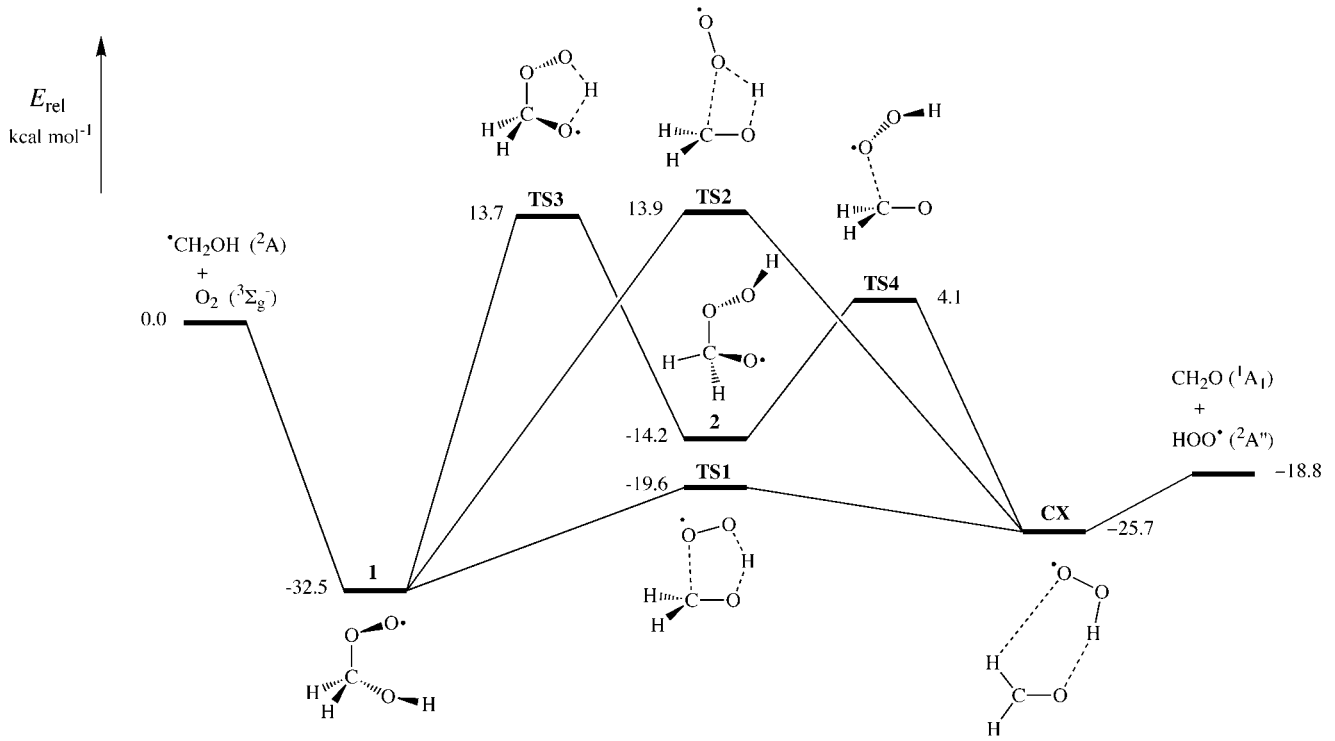

Figure 1. Schematic potential energy profiles showing the most relevant structures concerning the calculated pathways for the oxidation of $^{\bullet}CH_2OH$ by O_2 to form CH_2O and $HO_2^{\bullet}$. Relative energy values obtained from CCSD(T)/cc-pVTZ+ZPVE energy calculations at the CASSCF/6–311G(d,p)-optimized geometries.

Table 1. Calculated relative energies [kcal mol^{-1}] for various species through the $^{\bullet}CH_2OH+O_2$ reaction using the CASSCF/6–311G(d,p)-optimized geometries.

Species	ΔU[a]	$\Delta ZPVE$[b]	ΔE (0 K)	ΔH (298 K)	ΔG (298 K)
$CH_2OH^{\bullet}+O_2$	0.0	0.0	0.0	0.0	0.0
1	–37.8	5.3	–32.5	–33.9	–22.7
TS1	–20.9	1.3	–19.6	–21.2	–9.5
TS2	14.9	–1.0	13.9	12.9	22.7
TS3	13.3	0.4	13.7	11.9	23.9
2	–18.4	4.2	–14.2	–15.4	–4.5
TS4	2.3	1.8	4.1	3.0	13.6
CX	–27.4	1.7	–25.7	–25.8	–18.1
$H_2CO+HOO^{\bullet}$	–18.5	–0.3	–18.8	–18.7	–19.0

[a] Relative energy at the RCCSD(T)/cc-pVTZ level. [b] Differential zero-point vibracional energy corrections obtained from CASSCF/6–311G(d,p)-calculated harmonic vibrational frequencies.

Table 2. Calculated relative energies [kcal mol^{-1}] for various species through the $^{\bullet}CH_2OH+O_2$ reaction using the UB3LYP/6–311G(d,p)-optimized geometries

Species	ΔU[a]	$\Delta ZPVE$[b]	ΔE (0 K)	ΔH (298 K)	ΔG (298 K)
$CH_2OH^{\bullet}+O_2$	0.0	0.0	0.0	0.0	0.0
1	–35.0	4.8	–30.2	–31.6	–20.6
TS1	–21.2	0.8	–20.4	–22.1	–10.6
2	–16.2	2.9	–13.3	–14.6	–3.7
TS4	–2.8	2.2	–0.6	–1.9	8.9
CX	–26.0	2.0	–24.0	–24.4	–15.9
$H_2CO+HOO^{\bullet}$	–16.9	–0.2	–17.1	–17.1	–17.3

[a] Relative energy at the UB3LYP/cc-pVTZ level. [b] Differential zero-point vibrational energy corrections obtained from UB3LYP/6–311G(d,p)-calculated harmonic vibrational frequencies.

–37.5 eu obtained from the S(298 K) calculated at the CASSCF (Table S3 in the Supporting Information) and UB3LYP (Table S6 in the Supporting Information) levels of theory, respectively, are in reasonable agreement with the experimental $\Delta S_r(298\ K) = -35 \pm 1.0$ eu.[8]

We were not able to locate any transition structure for direct H-atom transfer from the OH group of $^{\bullet}CH_2OH$ to the O_2 leading to CH_2O and $HO_2^{\bullet}$. Thus it appears that the direct H-atom abstraction mechanism postulated[5b, 7] to be important at high temperatures does not occur on the ground state PES. This result is in sharp contrast with results from recent[47] high level ab initio calculations on the oxidation of the methoxy radical ($CH_3O^{\bullet}$) by O_2 ($^3\Sigma_g^-$) to generate CH_2O and $HO_2^{\bullet}$. Using RCCSD(T)/cc-pVTZ energies calculated for CASSCF/6-311G(d,p)-optimized geometries it was found that the oxidation of $CH_3O^{\bullet}$ occurs on the $^2A''$ PES through a direct H-atom transfer from this radical to the O_2 with a potential energy barrier ($\Delta U^{\neq}$) of 3.8 kcal mol^{-1}. This striking difference between the two isoelectronic reactions, $^{\bullet}CH_2OH+O_2$ and $CH_3O^{\bullet}+O_2$, is mainly ascribed to the much larger bond energy of the C–O bond as compared with that of the O–O bond, along with the larger bond energy of the O–H bond as compared with that of the C–H bond.[48]

Concerted $HO_2^{\bullet}$ elimination from peroxy radical 1: We have found two transition structures, **TS1** and **TS2** (Figure 2), for concerted $HO_2^{\bullet}$ elimination from **1**. The geometry of **TS1** is close to that of the transition structure reported by Evleth et al.[9] for the addition of $HO_2^{\bullet}$ to CH_2O to form **1**. Both **TS1** and **TS2** have a ringlike structure possessing a symmetry plane

0947-6539/01/0715-3380 $ 17.50+.50/0 *Chem. Eur. J.* **2001**, *7*, No. 15

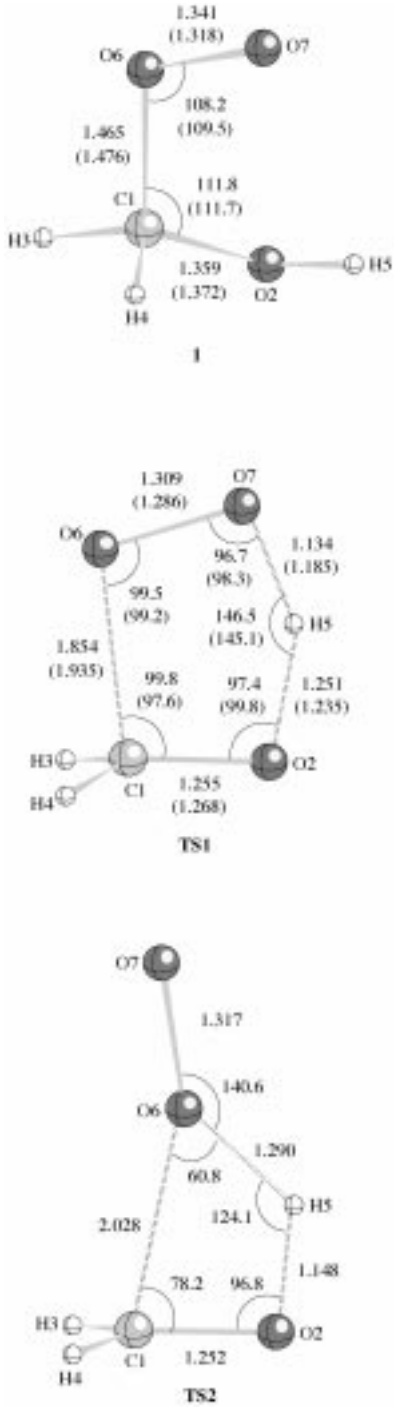

Figure 2. Selected parameters (distances [Å] and angles [°]) of the CASSCF/6–311G(d,p)-optimized geometries of the peroxy radical intermediate $^{\bullet}OOCH_2OH$ (**1**) and the transition structure (**TS1**) for the low-energy concerted $HO_2^{\bullet}$ elimination from $^{\bullet}OOCH_2OH$, and for the transition structure (**TS2**) for the high energy concerted $HO_2^{\bullet}$ elimination from $^{\bullet}OOCH_2OH$. The UB3LYP/6–311G(d,p) optimized geometric parameters are given in parentheses.[38] Other angles [°] for **1**: C1-O2-H5 109.7 (107.6), O2-C1-O6-O7 −65.8 (−61.0), H5-O2-C1-O6 70.4 (67.0).

(C_s molecular symmetry), the electronic state being $^2A''$. The IRC calculations at the CASSCF level of theory with the 6-311G(d,p) basis set showed that both **TS1** and **TS2** go backward to the peroxy radical **1**, and go forward to give a hydrogen-bonded $[H_2CO\cdots HOO^{\bullet}]$ complex, **CX** (Figure 3).

The concerted $HO_2^{\bullet}$ elimination from **1** through **TS1** is predicted to involve a 0 K activation energy ($\Delta E^{\ddagger}(0\,K)$) of 12.9 kcal mol^{-1} and a 298 K activation free-energy ($\Delta G^{\ddagger}(298\,K)$) of 13.2 kcal mol^{-1}. However, according to all

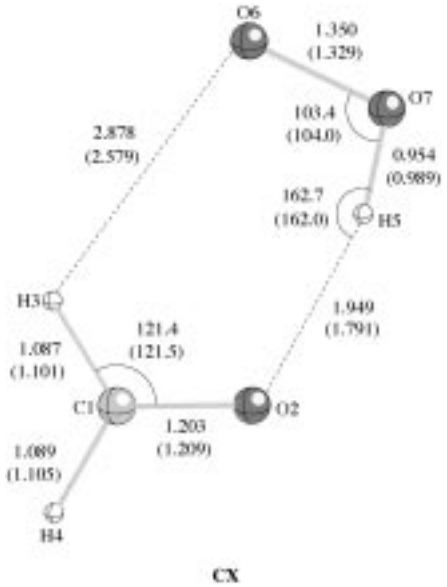

Figure 3. Selected parameters (distances [Å] and angles [°]) of the CASSCF/6–311G(d,p)-optimized geometries of the hydrogen-bonded $[H_2CO\cdots HOO^{\bullet}]$ complex (**CX**). The UB3LYP/6–311G(d,p) optimized geometric parameters are given in parentheses.[38]

relative energies (ΔU, ΔE, ΔH, and ΔG) shown in Table 1, **TS1** lies below the energy of the separated reactants of reaction (1). Thus the concerted $HO_2^{\bullet}$ elimination from **1**, which takes place through the addition/elimination mechanism via **TS1**, involves an overall $\Delta G^{\ddagger}(298\,K)$ of −9.5 kcal mol^{-1}. Therefore, the oxidation of $^{\bullet}CH_2OH$ by O_2 by this reaction pathway is predicted to be a quite feasible process under atmospheric conditions.

As expected for a concerted $HO_2^{\bullet}$ elimination from **1**, **TS1** involves the simultaneous breaking of the C−O bond and transfer of the hydrogen atom of the OH group to the terminal oxygen atom of **1**. Figure 4 displays the contour plot of the electronic charge density for **TS1** in the C_s symmetry plane. The presence of bond critical points between atom pairs C1−O6, O2−H5, and H5−O7 confirms that the breaking of the C1−O6 and O2−H5 bonds and the formation of the H5−O7 bond occur in a concerted mode. As noted by Evleth et al.,[9] a remarkable feature of **TS1** is that it is not of the "hydrogen abstraction by radicals" type. In order to illustrate this point, Figure 5 shows a diagrammatic representation of the electronic structure of the reactants, transition structure, and products for the concerted $HO_2^{\bullet}$ elimination from **1** through **TS1**. For simplicity **1** is assumed to be a doublet of A″ symmetry, originating from a coupling of the $^2A'$ state of $^{\bullet}CH_2OH$ with the $^3\Sigma_g^-$state of O_2. Following the convention of Goddard et al.[49] we have ignored the core orbitals, 1s for carbon, 1s and 2s for oxygen, which are tightly bound and remain relatively unchanged as the atoms are brought together to form the molecules. The dramatic, qualitative

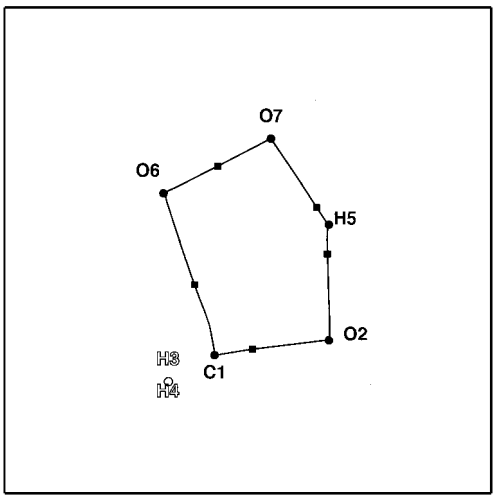

Figure 4. Contour plot in the C_s symmetry plane of the CASSCF/6–311G(d,p) electronic charge density of the transition structure **TS1**. Bond critical points are denoted by squares. The labels of the nuclei that lie in the C_s plane are bold and those that do not lie in this plane are open.

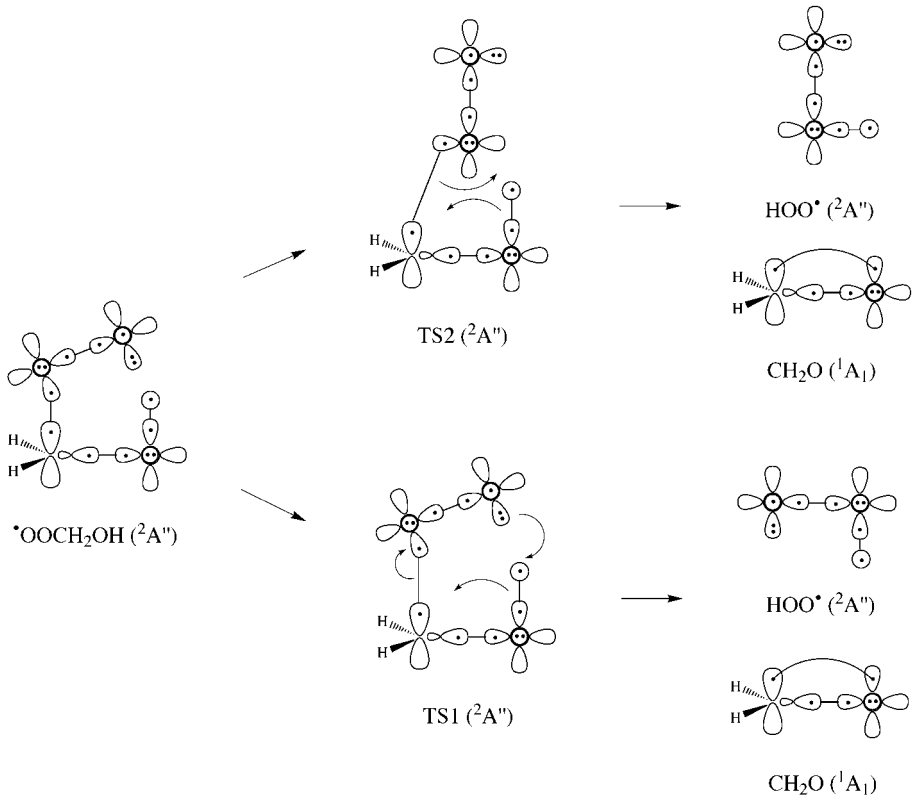

Figure 5. Diagrammatic representation of the electronic structures involved in the concerted $HO_2^{\bullet}$ elimination from **1** through **TS1**. The 1s orbital of the in-plane hydrogen is represented by ◯, the carbon and oxygen 2p orbitals are each represented by ∞ if in the plane of the paper and by ◯ if perpendicular to the plane of the paper, and the carbon sp hybrids are represented by ∞. Dots indicate the number of electrons in each orbital, tie lines indicate the coupling of two singly occupied orbitals into a bonding pair, and the curved arrows represent actual movement of both covalent and unshared electron pairs in reactions.

difference between **TS1** and the transition structures of free-radical H abstraction processes is that the singly occupied MO (SOMO) in **TS1** is antisymmetric (of a″ symmetry) with respect to the molecular plane of symmetry, because its electronic state is ^{2}A″, while the MO of the O–H bond implicated in the H-atom transfer is symmetric (of a′ symmetry) with respect this plane. Consequently, in **TS1** the SOMO and the latter MO are orthogonal and do not overlap. In other words, the H-atom transfer from the OH group to the OO• group cannot take place through an internal free-radical H-atom abstraction. From a qualitative point of view, the primary changes in bonding in **TS1** can be described as a formal shift of the unshared electron pair on the terminal oxygen atom (O7) to the hydrogen atom of the OH group, with the simultaneous shift of the electron pair of the O–H bond to the carbon and the shift of the electron pair of the C–O bond to the corresponding oxygen atom (O6). The odd electron is initially in the 2p orbital of a″ symmetry on the terminal oxygen atom and ends up in the 2p orbital of a″ symmetry on the adjacent oxygen atom after the H-atom transfer. Thus during the course of the reaction the odd electron remains the same. These electronic features indicate that the mechanism of the H-atom transfer in **1**, which leads to the concerted $HO_2^{\bullet}$ elimination through **TS1**, is an internal proton transfer rather than an intramolecular free-radical H-atom abstraction.

The main feature of **TS2** is that this transition structure involves the concerted breaking of the C–O bond and transfer of the H-atom of the OH group to the central oxygen atom of **1**. Figure 6 displays the contour plot of the electronic charge density for **TS2** in the C_s symmetry plane. The presence of bond critical points between atom pairs C1–O6, O2–H5, and H5–O6 confirms that the breaking of the C1–O6 and O2–H5 bonds and the formation of the H5–O6 bond occur in a concerted mode. A diagrammatic representation of the electronic structure of the reactants, transition structure, and products for the concerted $HO_2^{\bullet}$ elimination from **1** through **TS2** is given in Figure 5. As in the case of **TS1**, the electronic structure features of **TS2** indicate that the concerted $HO_2^{\bullet}$ elimination from **1** through **TS2** is an internal proton transfer rather than an intramolecular free-radical H-atom abstraction. The main difference between **TS1** and **TS2** is that **TS1** involves the concerted movement of two covalent electron pairs (the C1–O6 and H5–O2 bonds) and one unshared electron pair (on O7), whereas **TS2** implies only the movement of two covalent electron pairs (the C1–O6 and H5–O2 bonds).

0947-6539/01/0715-3382 $ 17.50+.50/0 *Chem. Eur. J.* **2001**, *7*, No. 15

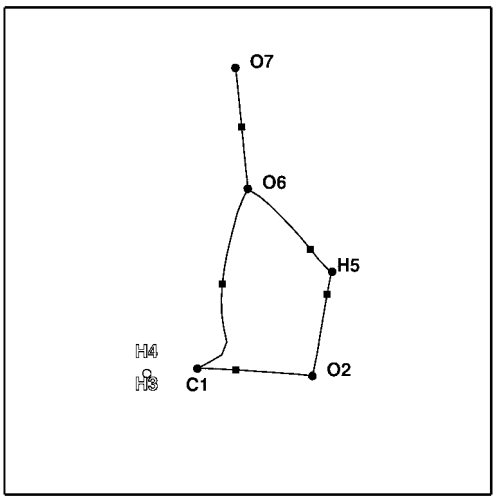

Figure 6. Contour plot in the C_s symmetry plane of the CASSCF/6–311G(d,p) electronic charge density of the transition structure **TS2**. Bond critical points are denoted by squares. The labels of the nuclei that lie in the C_s plane are bold and those that do not lie in this plane are open.

At the CASSCF/6-311G(d,p) level, **TS2** is calculated to be 34.4 kcal mol^{-1} more energetic than **TS1** (see Table S1 in the Supporting Information). This energy difference remains nearly the same (34.6 kcal mol^{-1}) at the UCCSD(T)/6-311G(d,p) level (see Table S2 in the Supporting Information), indicating that the dynamic valence-electron correlation does not significantly alter the relative energy of these transition structures. Furthermore, Table S2 shows that the basis extension also does not significantly change the relative energies of **TS1** and **TS2**. At the RCCSD(T)/cc-pVTZ level, **TS2** lies 35.8 kcal mol^{-1} above **TS1**. This large energy difference can be attributed primarily to the expected larger strain energy shown by the four-membered ringlike transition structure **TS2** as compared with the five-membered ringlike transition structure **TS1**. According to all relative energies (ΔU, ΔE, ΔH, and ΔG) shown in Table 1, **TS2** lies above the energy of the separated reactants of reaction (1). The concerted $HO_2^{\bullet}$ elimination from **1** via **TS2** involves a $\Delta G^{\neq}$(298 K) of 45.4 kcal mol^{-1}. At room temperature, this reaction pathway cannot compete with the concerted $HO_2^{\bullet}$ elimination from **1** through **TS1**, which involves a $\Delta G^{\neq}$(298 K) of 13.2 kcal mol^{-1}. However, the concerted $HO_2^{\bullet}$ elimination from **1** via **TS2** would be expected to be important at high temperatures.

The equilibrium geometry and the stabilization energy of complex **CX** (see Figure 3) calculated at the levels of theory used here have been reported recently.[47] Thus, at the RCCSD(T)/cc-pVTZ level, **CX** lies 8.9 kcal mol^{-1} below the energy of the isolated products CH_2O and $HO_2^{\bullet}$. Inclusion of the correction for the basis set superposition effects (BSSE), calculated with the counterpoise method,[50] leads to a stabilization energy of **CX** toward decomposition into CH_2O and $HO_2^{\bullet}$ of 8.1 kcal mol^{-1}. After addition of the thermal corrections to enthalpy this stabilization energy is reduced to 6.3 kcal mol^{-1} at 298 K. It is worth noting that **CX** corresponds to the hydrogen-bonded complex structure optimized at the UHF/6-31G(d) level, found on the reaction path taking $CH_2O+HO_2^{\bullet}$ to **1**, previously reported by Evleth et al.[9] These authors used the BACMP4/6-31G(d,p) method to compute a stabilization enthalpy of 8.0 kcal mol^{-1} at 300 K for the formation of this complex.

Stepwise $HO_2^{\bullet}$ elimination from peroxy radical 1: The first step of this pathway is the H-atom transfer from O2 to O7 in the peroxy radical **1** to form the alkoxy radical intermediate **2** (see Figure 1). Selected geometric parameters of the equilibrium structure calculated for **2** are shown in Figure 7. The formation of **2** can be viewed as an intramolecular H-atom

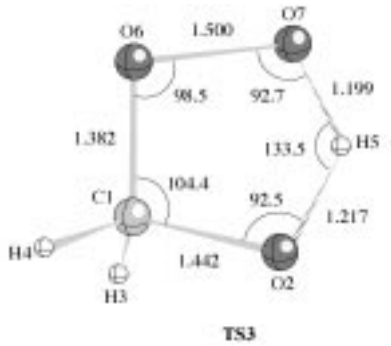

TS3

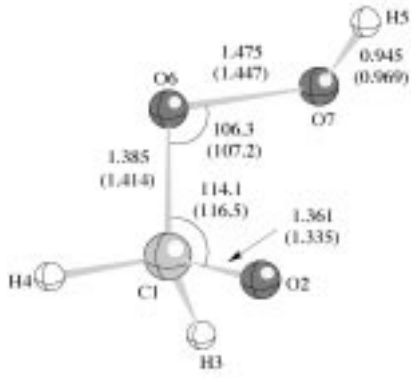

2

Figure 7. Selected parameters (distances [Å] and angles [°]) of the CASSCF/6–311G(d,p)-optimized geometries of the alkoxy radical intermediate $HOOCH_2O^{\bullet}$ (**2**) and the transition structure (**TS3**), connecting $^{\bullet}OOCH_2OH$ and $HOOCH_2O^{\bullet}$. The UB3LYP/6–311G(d,p) optimized geometric parameters are given in parentheses.[38] Other angles [°] for **TS3**: O2-C1-O6-O7 42.1, H5-O7-O6-C1 –34.8, H5-O2-C1-O6 –30.7; for **2**: O6-O7-H5 100.0 (101.0), O2-C1-O6-O7 70.9 (64.6), H5-O7-O6-C1 –107.5, H5-O2-C1-O6 (–87.6).

abstraction by the radical portion of the terminal oxygen in **1**. At the RCCSD(T)/cc-pVTZ+ZPVE level of computation this H-atom abstraction is predicted to be endoergic by 18.3 kcal mol^{-1}. Inclusion of the ΔH_c(298 K) value leads to a ΔH_r(298 K) value of 18.5 kcal mol^{-1} for the reaction **1** → **2**. However, the ΔH_r(298 K) value for the global process $^{\bullet}CH_2OH+O_2 \rightarrow$ **2** is –15.4 kcal mol^{-1}. A diagrammatic representation of the electronic structure of the reactants, transition structure, and products for the **1** → **2** rearrangement is given in Figure 8, where the curved semiarrows represent actual movement of single electrons. On the basis of the

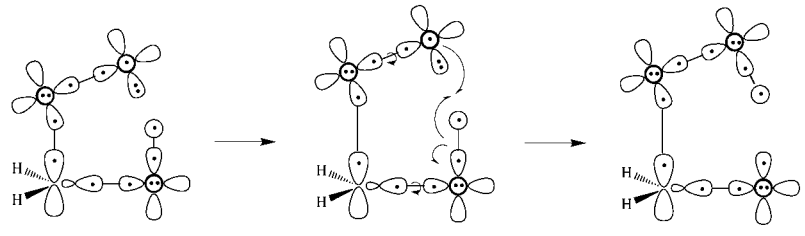

$^{\bullet}OOCH_2OH$ ($^2A''$) TS3 (^2A) $HOOCH_2O^{\bullet}$ (^2A)

Figure 8. Diagrammatic representation of the electronic structure of the reactants, transition structure, and products for **1** → **2**.

aforementioned orthogonality between the SOMO and the O–H bond in **1**, the H-atom transfer from the OH to the $OO^{\bullet}$ group cannot take place through a planar (C_s symmetry) transition structure. Consequently, the **1** → **2** rearrangement is found to take place via a puckered (C_1 symmetry) ringlike transition structure, **TS3** (Figure 7), this allows overlap between the 1s orbital of an H-atom of the OH group and the singly occupied 2p orbital of the terminal O atom. This H-atom abstraction in **1** leading to **2** through **TS3** involves a $\Delta E^{\neq}(0\ K)$ of 46.2 kcal mol^{-1}, which is much higher than that for the proton transfer in **1** that leads to **CX** through **TS1** ($\Delta E^{\neq}(0\ K) = 12.9$ kcal mol^{-1}). The main reason of this high activation energy is the formation of highly strained five-membered ring in going from **1** to the transition structure **TS3**. In fact, it is well known that the oxygen chain has an inherent tendency to assume a skew geometry in the hydrogen peroxides (RO_2H) in order to diminish lone pair repulsion between the O atoms.[51] Thus, the O7–H5 and O6–C1 bonds in the alkoxy radical intermediate **2**, formed after **TS3** is cleared are nearly perpendicular to the C1–O6–O7 plane, while in **TS3** these bonds are far from being perpendicular to this plane, as indicated by the H5–O7–O6–C1 and O2–C1–O6–O7 dihedral angles of $-34.8°$ and 42.1°, respectively. Furthermore, in **TS3** the O2–H5–O7 angle of 133.5° is smaller than that in **TS1** (146.5°).

The second step of the stepwise $HO_2^{\bullet}$ elimination from **1** is the simple homolytic cleavage of the C–O bond in **2**, which leads to the hydrogen-bonded [$H_2CO \cdots HOO^{\bullet}$] complex **CX**. This process is moderately exoergic, $\Delta E_r(0\ K) = -11.5$ kcal mol^{-1}, and takes place via the transition structure **TS4** (Figure 9) with a $\Delta E^{\neq}(0\ K)$ of 18.3 kcal mol^{-1}. Since at the RCCSD(T)/cc-pVTZ+ZPVE level of computation **TS3** is found to lie 27.9 kcal mol^{-1} above **2** in energy, it appears that the alkoxy radical intermediate **2** is a deep minimum on the PES.

In summary, the stepwise $HO_2^{\bullet}$ elimination from **1** has as the rate-determining step the formation of the radical intermediate **2** with a $\Delta G^{\neq}(298\ K)$ value of 46.6 kcal mol^{-1}. At room temperature this stepwise mechanism cannot compete with the concerted $HO_2^{\bullet}$ elimination from **1** through **TS1**, which involves a $\Delta G^{\neq}(298\ K)$ of 13.2 kcal mol^{-1}. However, the stepwise $HO_2^{\bullet}$ elimination from **1** would be expected to be important at high temperatures.

Comparison of the CASSCF and UB3LYP calculations: Overall, the structures calculated with the UB3LYP functional are similar to those optimized at the CASSCF level of theory. However, importantly we were able to compute neither **TS2** nor **TS3** by employing the UB3LYP functional with the 6-311G(d,p) basis set. We attempted to locate these two transition structures using as initial geometry that optimized at the CASSCF level of theory with the 6-311G(d,p) basis set.

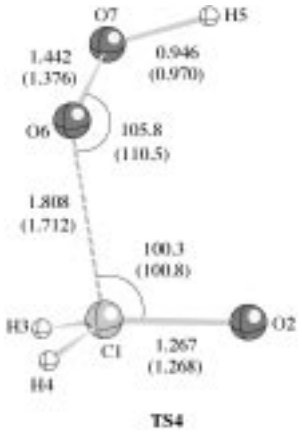

TS4

Figure 9. Selected parameters (distances [Å] and angles [°]) of the CASSCF/6–311G(d,p) optimized geometries of the transition structure (**TS4**) for the decomposition of $HOOCH_2O^{\bullet}$ into CH_2O and $HO_2^{\bullet}$. The UB3LYP/6–311G(d,p)-optimized geometric parameters are given in parentheses.[38] Other angles [°] for **TS4**: O6-O7-H5 101.4 (102.9), O2-C1-O6-O7 72.3 (80.3), H5-O7-O6-C1 −94.9 (−115.3).

The optimization process led to the previously found transition structure **TS1** in each case. These unexpected results prompted us to compute **TS1**, **TS2**, and **TS3** at the UMP2 and UCISD levels of theory with the 6-311G(d,p) basis set starting at the corresponding CASSCF/6-311G(d,p) optimized structure. In each case we obtained a transition structure close to that computed at the CASSCF level of theory. Therefore, both the UMP2 and UCISD calculations confirm the existence of the **TS1**, **TS2**, and **TS3** transition structures on the ground-state PES of the $^{\bullet}CH_2OH+O_2$ reaction.

Apparently, the DFT calculations based on the UB3LYP functional correctly describe the electronic structure of the lowest energy transition structure **TS1** but not those of the two high energy transition structures **TS2** and **TS3**. A similar failure of the UB3LYP functional was also observed[47] in a recent theoretical study of the oxidation of $CH_3O^{\bullet}$ by O_2, in which the transition structure for the 1,4-hydrogen shift in $CH_3OOO^{\bullet}$, which leads to $^{\bullet}CH_2OOOH$, could not be located with the UB3LYP method despite being computed at the CASSCF and UCISD levels of theory. Consequently, we recommend some caution in the use of the UB3LYP functional for computing intramolecular H-atom transfer reactions of free radicals.

Finally, it is worth noting that the relative energies obtained from the UB3LYP/cc-pVTZ calculations in conjunction with

  0947-6539/01/0715-3384 $ 17.50+.50/0 *Chem. Eur. J.* **2001**, *7*, No. 15

the UB3LYP/6-311G(d,p) geometries and harmonic vibrational frequencies (Table 2) for the concerted $HO_2^{\bullet}$ elimination from **1** are in reasonable agreement with those obtained from the RCCSD(T)/cc-pVTZ calculations based on the CASSCF/6-311G(d,p) geometries and harmonic vibrational frequencies (Table 1). In particular, from the $\Delta E(0\,K)$ value given in Table 2 we obtain an activation energy of 9.8 kcal mol^{-1} and a reaction energy of 6.2 kcal mol^{-1} for the pathway **1** → **TS1** → **CX**. These values are 3.1 and 0.6 kcal mol^{-1} lower than the $\Delta E^{\neq}(0\,K) = 12.9$ kcal mol^{-1} and $\Delta E_r(0\,K) = 6.8$ kcal mol^{-1}, respectively, determined from the $\Delta E(0\,K)$ value given in Table 1.

Conclusion

The reaction mechanisms of the hydroxymethyl radical oxidation by molecular oxygen in the gas-phase were studied by means of high-level quantum-chemical electronic structure calculations. The CASSCF method with the 6-311G(d,p) basis set was used to optimize the geometry of nine stationary points on the ground-state potential energy reaction surface and to compute their harmonic vibrational frequencies. Relative energies were calculated at the CCSD(T) level of theory with extended basis sets up to cc-pVTZ using the CASSCF/6-311G(d,p) optimized geometries. The energetics were further corrected for zero-point and temperature effects. The calculations indicate that the oxidation of $^{\bullet}CH_2OH$ by O_2 is a stepwise process starting with the barrier-free formation of the peroxy radical $^{\bullet}OOCH_2OH$ with a $\Delta G(298\,K)$ value of -22.7 kcal mol^{-1}. In contrast with earlier studies suggesting that a direct H-atom abstraction mechanism might occur at high temperatures, we could not find any transition structure for direct H-atom transfer from the OH group of $^{\bullet}CH_2OH$ to the O_2.

Contrary to the generally accepted rearrangement/decomposition mechanism, the lowest energy pathway connecting $^{\bullet}OOCH_2OH$ with the observed products CH_2O and $HO_2^{\bullet}$ is predicted to be a concerted $HO_2^{\bullet}$ elimination from $^{\bullet}OOCH_2OH$ through a five-membered ringlike transition structure **TS1** of C_s symmetry with a $\Delta G^{\neq}(298\,K)$ value of 13.2 kcal mol^{-1}. A higher energy pathway involving a four-membered ringlike transition structure **TS2** of C_s symmetry with a $\Delta G^{\neq}(298\,K)$ value of 45.4 kcal mol^{-1} was also found for the concerted $HO_2^{\bullet}$ elimination from $^{\bullet}OOCH_2OH$. An analysis of the electronic structure of **TS1** and **TS2** indicates that both modes of concerted $HO_2^{\bullet}$ elimination are better described as internal proton transfers rather than intramolecular free-radical H-atom abstractions.

The stepwise $HO_2^{\bullet}$ elimination from $^{\bullet}OOCH_2OH$ involves an intramolecular 1,4-H-atom transfer yielding the alkoxy radical intermediate $HOOCH_2O^{\bullet}$, which decomposes to form the products CH_2O and $HO_2^{\bullet}$. The intramolecular 1,4-H-atom transfer is the rate-determining step and takes place via a puckered ringlike transition structure **TS3** with a $\Delta G^{\neq}(298\,K)$ of 46.6 kcal mol^{-1}.

The oxidation of $^{\bullet}CH_2OH$ by O_2, which takes place through the addition/elimination mechanism via **TS1**, is predicted to involve an overall $\Delta G^{\neq}(298\,K)$ value of -9.5 kcal mol^{-1}, whereas the addition/elimination mechanism via **TS2** and the addition/rearrangement/decomposition mechanism via **TS3** are predicted to involve overall $\Delta G^{\neq}(298\,K)$ values of 22.7 and 23.9 kcal mol^{-1}, respectively. Therefore, it can be concluded that at low and room temperatures the latter two reaction pathways cannot compete with the addition/elimination pathway via **TS1**. However, the addition/elimination pathway via **TS2** and the addition/rearrangement/decomposition pathway would be expected to be important at high temperatures.

The observed non-Arrhenius behavior of the rate constant temperature dependence for the gas-phase oxidation of $^{\bullet}CH_2OH$ might be ascribed to the combined effect of the initial barrier-free formation of the $^{\bullet}OOCH_2OH$ adduct with a free energy (at 298 K) release of 22.7 kcal mol^{-1} and the existence of a low-barrier and two high-barrier pathways for its decomposition into the products CH_2O and $HO_2^{\bullet}$. Thus, the observed decrease of the rate constant below room temperature and also slightly above room temperature are a consequence of the initial formation of the vibrationally excited $^{\bullet}OOCH_2OH$ adduct, which can dissociate back to reactants or undergo concerted $HO_2^{\bullet}$ elimination through a transition structure (**TS1**) whose free energy (at 298 K) value is 9.5 kcal mol^{-1} lower than the sum of the free energies of the separated reactants. At temperatures around 298 K the apparent rate constant for the $HO_2^{\bullet}$ elimination channel would be expected to level off and then decrease as the dissociation back to reactants continued to increase. The fact that at high temperatures the rate constant is observed to increase rapidly with increasing temperature suggests that the $HO_2^{\bullet}$ elimination from $^{\bullet}OOCH_2OH$ becomes more competitive with its dissociation back to the reactants because at high temperatures the $HO_2^{\bullet}$ elimination can also occur through the high energy transition structures **TS2** and **TS3.**

Acknowledgements

This research was supported by the Spanish DGICYT (Grant PB98-1240-CO2-01). Additional support came from Catalonian CIRIT (Grant 1999SGR00043). Calculations described in this work were performed on a HP9000 J282 workstation at the Universitat de Barcelona and on the IBM SP2 at the Centre de Supercomputació de Catalunya (CESCA). We acknowledge gratefully the MRDCI calculations of Dr. J. M. Anglada (CSIC), which allowed the selection of the active space used in our CASSCF calculations.

[1] H. Niki, P. D. Maker, C. M. Savage, L. P. Breitenbach, *Chem. Phys. Lett.* **1981**, *80,* 499.
[2] For a review, see: R. Atkinson, *Atmos. Environ. A* **1990**, *24*, 1.
[3] C. K. Westbrook, F. L. Dryer, *Combustion Sci. Technol.* **1979**, *20*, 215.
[4] S. Dóbé, F. Temps, T. Böhland, H. G. Wagner, *Z. Naturforsch. A* **1985**, *40*, 1289.
[5] a) H.-H. Gotheer, G. Riekert, U. Meier, T. Just, *Ber. Bunsen-Ges. Phys. Chem.* **1985**, *89,* 187; b) H.-H. Gotheer, G. Riekert, D. Walter, T. Just, *J. Phys. Chem.* **1988**, *92,* 4028.
[6] W. A. Payne, J. Brunning, M. B. Mitchell, L. J. Stief, *Int. J. Chem. Kinet.* **1988**, *20*, 63.
[7] F. L. Nesbitt, W. Payne, L. J. Steif, *J. Phys. Chem.* **1988**, *92*, 4030.
[8] B. Veyret, R. Lesclaux, M. T. Rayez, J. C. Rayez, R. A. Cox, K. G. Moortgat, *J. Phys. Chem.* **1989**, *93,* 2368.

  0947-6539/01/0715-3385 $ 17.50+.50/0

[9] E. M. Evleth, C. F. Melius, M. T. Rayez, J. C. Rayez, W. Forst, *J. Phys. Chem.* **1993**, *97,* 5040.
[10] J. A. Pople, R. K. Nesbet, *J. Chem. Phys.* **1954**, *22*, 571.
[11] a) W. J. Hehre, R. Ditchfield, J. A. Pople, *J. Chem. Phys.* **1972**, *56*, 2257; b) P. C. Hariharan, J. A. Pople, *Theor. Chim. Acta*. **1973**, *28*, 213.
[12] H. B. Schlegel, *J. Comput. Chem*. **1982**, *3,* 214.
[13] J. M. Bofill, *J. Comput. Chem.* **1994**, *15,* 1.
[14] M. J. Frisch, G. W. Trucks, H. B. Schlegel, P. M. W. Gill, B. G. Johnson, M. A. Robb, J. R. Cheeseman, T. A. Keith, G. A. Petersson, J. A. Montgomery, K. Raghavachari, M. A. Al-Laham, V. G. Zakrzewski, J. V. Ortiz, J. B. Foresman, J. Cioslowski, A. Stefanov, A. Nanayakkara, M. Challacombe, C. Y. Peng, P. Y. Ayala, W. Chen, M. W. Wong, J. L. Andres, E. S. Replogle, R. Gomperts, R. L. Martin, D. J. Fox, J. S. Binkley, D. J. Defrees, J. Baker, J. J. P. Stewart, M. Head-Gordon, C. Gonzalez, J. A. Pople, Gaussian, Inc., Pittsburgh (PA), USA, **1995**.
[15] For a review, see :B. O. Roos, *Adv. Chem. Phys*. **1987**, *69*, 399.
[16] R. Krishnan, J. S. Binkley, J. A. Pople, *J. Chem. Phys.* **1980**, *72,* 650.
[17] a) J. Baker, *J. Comput. Chem.* **1986**, *7,* 385; b) J. Baker, *J. Comput. Chem.* **1987**, *8,* 563.
[18] J. M. Anglada, J. M. Bofill, *Chem. Phys. Lett.* **1995**, *243*, 151.
[19] M. W. Schmidt, K. K. Baldrige, J. A. Boatz, S. T. Elbert, M. S. Gordon, J. Jensen, S. Koseki, N. Matsunaga, K. A. Nguyen, S. Su, T. L. Windus, M. Dupuis, J. A. Montgomery, *J. Comput. Chem.* **1993**, *14*, 1347.
[20] K. Fukui, *Acc. Chem. Res.* **1981**, *14,* 363.
[21] C. Gonzalez, H. B. Schlegel, *J. Chem. Phys.* **1989**, *90,* 2154; b) C. Gonzalez, H. B. Schlegel, *J. Phys. Chem.* **1990**, *94,* 5523.
[22] a) A. D. Becke, *Phys. Rev. A* **1988**, *37,* 3098; b) A. D. Becke, *J. Chem. Phys.* **1993**, *98*, 5648.
[23] C. Lee, W. Yang, R. G. Parr, *Phys. Rev. B* **1988**, *37,* 785.
[24] P. J. Stevens, F. J. Devlin, C. F. Chablowski, M. J. Frisch, *J. Phys. Chem.* **1994**, *98,* 11623.
[25] a) C. Møller, M. Plesset, *Phys. Rev.* **1934**, *46*, 618; b) J. A. Pople, J. S. Binkley, R. Seeger, *Int. J. Quantum Chem. Symp.* **1976**, *10*, 1; c) R. Krishnan, J. A. Pople, *Int. J. Quantum Chem.* **1978**, *14*, 91.
[26] J. A. Pople, R. Seeger, R. Krishnan, *Int. J. Quantum. Chem. Symp.* **1977**, *11,* 149.
[27] For a review, see R. J. Bartlett, *J. Phys. Chem.* **1989**, *93*, 1697.
[28] K. Raghavachari, G. W. Trucks, J. A. Pople, M. Head-Gordon, *Chem. Phys. Lett.* **1989**, *157,* 479.
[29] M. J. Frisch, J. A. Pople, J. S. Binkley, *J. Chem. Phys.* **1984**, *80,* 3265.
[30] T. H. Dunning, *J. Chem. Phys.* **1989**, *90,* 1007.
[31] P. J. Knowles, C. Hampel, H.-J. Werner, *J. Chem. Phys.* **1993**, *99*, 5219.
[32] a) G. D. Purvis, R. J. Bartlett, *J. Chem. Phys.* **1982**, *76*, 1910; b) C. Hampel, K. A. Peterson, H.-J. Werner, *Chem. Phys. Lett.* **1992**, *190,* 1; c) M. J. O. Deegan, P. J. Knowles, *Chem. Phys. Lett.* **1994**, *227*, 321.
[33] H.-J. Werner, P. J. Knowles, J. Almlöf, R. D. Amos, A Berning, D. L. Cooper, M. J. O. Deegan, A. J. Dobbyn, S. T. Eckert, C. Hampel, C. Leininger, R. Lindh, W. Meyer, M. E. Mura, A. Nicklass, P. Palmeiri, K. A. Peterson, R. Pitzer, P. Pulay, G. Rauhaut, M. Schuetz, H. Stoll, A. J. Stone, T. Thorsteinsson, University of Stuttgart, Germany, **1998**.
[34] For example, see: D. McQuarrie, *Statistical Mechanics,* Harper and Row, New York, **1986**.
[35] R. F. W. Bader, *Atoms in Molecules: A Quantum Theory,* Clarendon, Oxford, **1990**.
[36] a) F. W. Biegler-König, R. F. W. Bader, T.-H. Tang, *J. Comput. Chem.* **1982**, *3,* 317; b) R. F. W. Bader, T.-H. Tang, Y. Tal, F. W. Biegler-König, *J. Am. Chem. Soc.* **1982**, *104*, 946.
[37] a) P. L. A. Popelier, R. G. A. Bone, UMIST, Manchester, UK, **1997**; b) P. L. A. Popelier, *Comput. Phys. Commun.* **1998**, *108,* 180.
[38] Full set of Cartesian coordinates for all stationary points as obtained by the different methods are available upon request from the corresponding author.
[39] $\Delta H_{f,298}(^{\bullet}CH_2OH) = -4.4 \pm 1.0$ (ref. [40]), $\Delta H_{f,298}(HO_2^{\bullet}) = 3.5$ (ref. [41]), and $\Delta H_{f298}(CH_2O) = -26.0 \pm 0.2$ kcal mol^{-1} (ref. [42]).
[40] J. Berkowitz, G. B. Ellison, D Gutman, *J. Chem. Phys.* **1994**, *98,* 274.
[41] S. W. Benson, *J. Phys. Chem.* **1996**, *100*, 13544.
[42] S. G. Lias, J. E. Bartmess, J. B. Liebman, J. L. Holmes, R. D. Levin, W. G. Mallard, *J. Phys. Chem. Ref. Data* **1988**, *17*, 168.
[43] S. P. Walch, *Chem. Phys. Lett.* **1993**, *215,* 81.
[44] E. Sicilia, F. P. DiMaio, N. Russo, *Chem. Phys. Lett.* **1994**, *225,* 208.
[45] W. H. Green, *Int. J. Quantum. Chem.* **1994**, *52,* 837.
[46] B. S. Jursic, *J. Phys. Chem. A* **1997**, *101,* 2345.
[47] J. M. Bofill, S. Olivella, A. Solé, J. M. Anglada, *J. Am. Chem. Soc.* **1999**, *121,* 1337.
[48] The experimental average bond energies of the C−O, O−O, O−H, and C−H single bonds are 84.0, 33.2, 110.6, and 98.8 kcal mol^{-1}, respectively. See C. W. N. Cumper, *Wave Mechanics for Chemists,* Heinemann, London, **1966**, p. 219.
[49] W. A. Goddard III, T. H. Dunning, W. J. Hunt, P. J. Hay, *Acc. Chem. Res.* **1973**, *6*, 368.
[50] S. F. Boys, F. Bernardi, *Mol. Phys.* **1970**, *19,* 553.
[51] For a review, see :D. J. Mckay, J. S. Wright, *J. Am. Chem. Soc.* **1998**, *120,* 1003.

Received: December 13, 2000
Revised: March 12, 2001 [F2932]

  0947-6539/01/0715-3386 $ 17.50+.50/0